JOURNAL OF GEOPHYSICAL RESEARCH, VOL. 112, D21202, doi:10.1029/2007JD008464, 2007

Chemical and physical characteristics of nascent aerosols produced by bursting bubbles at a model air-sea interface

William C. Keene,[1] Hal Maring,[2] John R. Maben,[1] David J. Kieber,[3] Alexander A. P. Pszenny,[4] Elizabeth E. Dahl,[3,5] Miguel A. Izaguirre,[6] Andrew J. Davis,[3] Michael S. Long,[1] Xianliang Zhou,[7] Linda Smoydzin,[8,9] and Rolf Sander[10]

Received 26 January 2007; revised 8 May 2007; accepted 12 July 2007; published 3 November 2007.

[1] Breaking waves on the ocean surface produce bubbles that, upon bursting, inject seawater constituents into the atmosphere. Nascent aerosols were generated by bubbling zero-air through flowing seawater within an RH-controlled chamber deployed at Bermuda and analyzed for major chemical and physical characteristics. The composition of feed seawater was representative of the surrounding ocean. Relative size distributions of inorganic aerosol constituents were similar to those in ambient air. Ca^{2+} was significantly enriched relative to seawater (median factor = 1.2). If in the form of $CaCO_3$, these enrichments would have important implications for pH-dependent processes. Other inorganic constituents were present at ratios indistinguishable from those in seawater. Soluble organic carbon (OC) was highly enriched in all size fractions (median factor for all samples = 387). Number size distributions exhibited two lognormal modes. The number production flux of each mode was linearly correlated with bubble rate. At 80% RH, the larger mode exhibited a volume centroid of ~5-μm diameter and included ~95% of the inorganic sea-salt mass; water comprised 79% to 90% of volume. At 80% RH, the smaller mode exhibited a number centroid of 0.13-μm diameter; water comprised 87% to 90% of volume. The median mass ratio of organic matter to sea salt in the smallest size fraction (geometric mean diameter = 0.13 μm) was 4:1. These results support the hypothesis that bursting bubbles are an important global source of CN and CCN with climatic implications. Primary marine aerosols also influence radiative transfer via multiphase processing of sulfur and other climate-relevant species.

Citation: Keene, W. C., et al. (2007), Chemical and physical characteristics of nascent aerosols produced by bursting bubbles at a model air-sea interface, *J. Geophys. Res.*, *112*, D21202, doi:10.1029/2007JD008464.

1. Introduction

[2] Breaking waves on the ocean surface produce bubbles that, upon bursting, inject seawater constituents into the overlying atmosphere via both jet drop and film drop formation [*Blanchard and Woodcock*, 1980]. The nascent droplets dehydrate into equilibrium with ambient water vapor and undergo other multiphase transformations involving the scavenging of gases, aqueous and surface reactions, and volatilization of products that influence important, interrelated chemical and physical processes in the Earth's atmosphere. Acid displacement reactions involving HCl regulate aerosol pH and associated pH-dependent chemical pathways [*Keene et al.*, 1998, 2004]. The production from ionic marine-derived precursors and multiphase cycling of halogen radicals represents a significant net sink for ozone in the remote marine boundary layer (MBL) [*Dickerson et al.*, 1999; *Galbally et al.*, 2000; *Nagao et al.*, 1999; *Sander et al.*, 2003; *Pszenny et al.*, 2004] and a potentially important net source under polluted conditions [*Tanaka et al.*, 2003]. The formation and scavenging of halogen nitrates accel-

[1]Department of Environmental Sciences, University of Virginia, Charlottesville, Virginia, USA.
[2]Radiation Sciences Program, NASA, Washington, D. C., USA.
[3]Chemistry Department, College of Environmental Science and Forestry, State University of New York, Syracuse, New York, USA.
[4]Institute for the Study of Earth, Oceans, and Space, University of New Hampshire, Durham, New Hampshire, USA.
[5]Now at Chemistry Department, Loyola College in Maryland, Baltimore, Maryland, USA.
[6]Rosenstiel School of Marine and Atmospheric Science, University of Miami, Miami, Florida, USA.
[7]Wadsworth Center, New York State Department of Health, and School of Public Health, State University of New York, Albany, New York, USA.
[8]Institute for Environmental Physics, University of Heidelberg, Heidelberg, Germany.
[9]Now at School of Environmental Sciences, University of East Anglia, Norwich, UK.
[10]Air Chemistry Department, Max Planck Institute for Chemistry, Mainz, Germany.

0148-0227/07/2007JD008464$09.00

erates the conversion of NO_x to HNO_3 and particulate NO_3^- and thereby contribute to net O_3 destruction [*Sander et al.*, 1999]. BrO and atomic Cl oxidize $(CH_3)_2S$ in the gas phase [*Toumi*, 1994; *Keene et al.*, 1996; *Saiz-Lopez et al.*, 2004] and ozone and hypohalous acids oxidize S(IV) in aerosol solutions [*Vogt et al.*, 1996], which influence sulfur cycling and related effects on radiative transfer and climate [*von Glasow et al.*, 2002; *von Glasow and Crutzen*, 2004]. The photochemical processing of marine-derived organic compounds is an important source of OH and other radicals that enhance oxidation potential within aerosol solutions [*McDow et al.*, 1996; *Davis et al.*, 2006; *Anastasio and Newberg*, 2007; X. Zhou et al., Photochemical production of hydroxyl radicals and peroxides in nascent marine aerosols, unpublished manuscript, 2007, hereinafter referred to as Zhou et al., unpublished manuscript, 2007]. Marine aerosols also influence Earth's climate directly by scattering and absorbing solar radiation and indirectly by regulating the microphysical properties and corresponding albedo of clouds [*Intergovernmental Panel on Climate Change*, 2001]. Because many marine-derived organic compounds suppress surface tension, their incorporation into marine aerosols may reduce the supersaturation required to activate particles into cloud droplets [e.g., *Decesari et al.*, 2005]. Thus a potentially important direct coupling exists between marine-derived organic material, cloud microphysics, and climate feedback. However, nascent aerosols are rapidly (seconds) modified via interaction with light and reactive trace gases in marine air [e.g., *Chameides and Stelson*, 1992; *Erickson et al.*, 1999; *Sander et al.*, 2003]. In addition, fresh aerosols are injected into an atmosphere already populated with a mixture of mechanically produced marine aerosols of various ages and associated degrees of modification, primary aerosols that originate from nonmarine sources (crustal dust, graphic carbon, etc.) and associated reaction products, and secondary aerosols produced via nucleation and growth pathways. Consequently, it is virtually impossible to unequivocally characterize primary marine constituents on the basis of measurements of aerosol composition in ambient air.

[3] Various lines of evidence suggests that, relative to seawater, chemical fractionation of the major inorganic constituents (including Na^+, Mg^{2+}, Ca^{2+}, K^+, Cl^-, and SO_4^{2-}) during the mechanical production of marine aerosols is limited to a few percent if it occurs as all [*Duce and Hoffman*, 1976; *Keene et al.*, 1986]. In contrast, chamber experiments [*Hoffman and Duce*, 1976; *Tseng et al.*, 1992] and field observations [*Chesselet et al.*, 1981; *Middlebrook et al.*, 1998; *O'Dowd et al.*, 2004] suggest that marine-derived organic constituents are highly enriched during aerosol production. Scavenging of surface-active organic material from bulk seawater and its transport to the air-sea interface by rising bubbles is well documented [*Blanchard and Syzdek*, 1974; *Blanchard*, 1975; *Hoffman and Duce*, 1976; *Wallace and Duce*, 1978; *Skop et al.*, 1991; *Tseng et al.*, 1992]. The walls of subsurface bubbles are coated with organic microlayers consisting of soluble and insoluble compounds concentrated from bulk seawater [e.g., *Clift et al.*, 1977; *Rosen*, 1978; *Scott*, 1986]. When bubbles burst at the ocean surface, organics concentrated on their walls are injected into the atmosphere along with dissolved inorganic and organic constituents of seawater and entrained particulates. Chamber experiments indicate that the sea-to-air flux of organics via bubble bursting increases with the increasing path length of rising bubbles [*Hoffman and Duce*, 1976] and with increasing bubble rate and decreasing bubble size [*Tseng et al.*, 1992]. In addition, the sea-to-air flux is proportional to the rate at which the surfactants are delivered to the surface by rising bubbles [*Tseng et al.*, 1992]. Organic carbon associated with the microlayer at the air-sea interface is also injected into the atmosphere during aerosol production [*Bezdek and Carlucci*, 1974; *Gershey*, 1983; *Leck and Bigg*, 2005]. However, the reported carbon enrichments in the surface microlayer are generally small (<10 [e.g., *Hunter*, 1997]) compared to those in marine aerosols (>100), which (together with results of studies summarized above) suggest that contributions from the microlayer probably account for relatively minor fractions of the injected carbon under most conditions.

[4] In addition to uncertainties about chemical composition of nascent, mechanically produced marine aerosols, the associated number size distributions and related hygroscopic properties are also uncertain. Most inorganic mass (~95%) is typically associated with super-μm diameter size fractions but sub-μm fractions dominate corresponding number concentrations [e.g., *Blanchard and Syzdek*, 1988; *Resch and Afeti*, 1991, 1992; *O'Dowd et al.*, 1997; *Mårtensson et al.*, 2003; *Clarke et al.*, 2006]. Several investigations based on measurements of ambient aerosols suggest that film drops from bursting bubbles produce high number concentrations of primary, sub-μm, organic-rich particles with potentially important implications for cloud properties and climate feedback [*Middlebrook et al.*, 1998; *O'Dowd et al.*, 2004; *Leck and Bigg*, 2005; *Lohmann and Leck*, 2005]. As discussed above, however, the rapid (seconds) chemical evolution [*Chameides and Stelson*, 1992; *Erickson et al.*, 1999] and long atmospheric lifetimes (many days) of sub-μm aerosols coupled with the current lack of rapid, specific, and conservative measurement techniques for sea-salt and organic constituents over the full relevant size range seriously constrain resolution in deconvoluting relative contributions from primary marine, nonmarine, and secondary (e.g., condensation) sources based on measurements in ambient air.

[5] In this study, we generated primary marine aerosols by bubbling zero air through flowing seawater under controlled conditions within an enclosed Pyrex and Teflon chamber. Size distributions of inorganic and organic constituents and corresponding number concentrations in the overlying air were measured simultaneously over a range of relative humidity (RH). By eliminating all other primary and secondary sources of particulate material, the chemical and physical characteristics of nascent, size-resolved aerosols produced by bursting bubbles at the model air-sea interface could be evaluated unequivocally. Companion papers evaluate the photochemical processing of marine-derived OC associated with nascent aerosols, the associated production of OH and hydroperoxides, and related implications for multiphase chemical evolution of

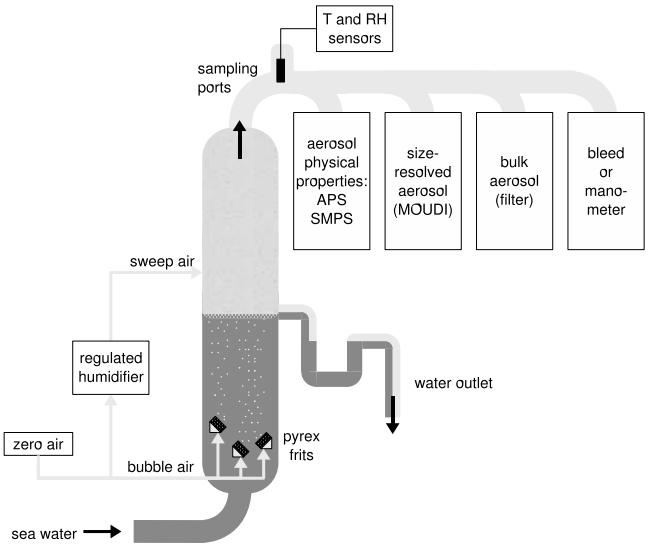

Figure 1. Schematic diagram of aerosol generator.

marine air [*Davis et al.*, 2006; Zhou et al., unpublished manuscript, 2007].

2. Methods

[6] A high-capacity aerosol generator similar in design to the low-capacity apparatus reported by *Hoffman and Duce* [1976] was fabricated from commercial Pyrex glassplant components (Sentinal Process Systems Inc., Hatboro, PA, Figure 1 and Table 1). The body consisted of 20-cm-inner-diameter (ID) pipe sections connected with Teflon-lined flange/gasket assemblies. Pyrex ports were added to pass air, water, and samples and to mount sensors. All interior surfaces were Pyrex or Teflon that had been washed with 10% HCl and thoroughly rinsed with low-organic-carbon ($\sim$4 μM C) Type 1 deionized water (>18.3 MΩ cm; DIW) prior to deployment. Fresh, unfiltered seawater flowed from bottom to top (range of 4 to 10 L min^{-1}) and six 2.54-cm-ID overflow ports maintained constant water depth of 133 cm; a trap prevented lab-air exchange at the exhaust. The depth of air in the overlying headspace was 81.3 cm. Zero air was bubbled (range of 1.0 to 9.0 L min^{-1}) through eleven, 90-mm-diameter, fine-porosity (E) glass frits (Ace part number 7176-61) clustered in three, independently regulated groups positioned over a depth range between approximately 130 and 100 cm below the air-water interface (Figure 1). Visual inspection indicated that bubble lifetimes ranged from about 7 to 15 seconds; bubble sizes near the air-water interface ranged from about 200- to 600-μm diameter; and, depending on bubble flow rate, the water surface was covered to varying degrees by bubble rafts. The depths of bubble clouds from breaking waves on the ocean surface typically range from 100 to 300 cm and sometimes more; depth generally increases with increasing wind speed [*Thorpe*, 1982; *Thorpe et al.*, 1982; *Thorpe and Hall*, 1983]. On the basis of these observations, we infer that the average injection depth and the associated lifetimes of bubbles in the generator were reasonably representative of average conditions for the surface ocean.

[7] Zero (sweep) air was hydrated with DIW immediately upstream of the generator by pumping through three mist chamber assemblies positioned in tandem. The hydrated sweep air entered the generator through three 2.54-cm-ID ports centered 24 cm above the water surface. The exterior temperatures of the mist chamber walls and corresponding rates of DIW evaporation were manually adjusted with Variac-controlled heat tape to maintain a specified RH (range of 33% to 95%) at the outlet of the generator; adjustments in RH had no detectable influence on air temperature within the generator. The combined flow rates of sweep plus bubble air ranged from 40 to 78 L min^{-1}. Aerosol-laden exhaust air was sampled for chemical and physical characterization through Pyrex ports at the top of the generator and transferred to instruments under laminar flow; the calculated transmission efficiency for 20-μm-diameter particles was 95%. To prevent contamination by room air, the generator was operated under slight positive pressure by maintaining the sweep-air flow several L min^{-1} greater than the combined sampling rate minus the bubbling rate; excess air was vented through a 1-way ''flutter'' valve at the top. Airflow rates were regulated with needle valves and quantified with Teledyne Hastings mass flowmeters. Seawater flow rates were measured at the exhaust. RH and temperature were measured continuously at the outlet (Figure 1) with a Vasala model HMP 233 probe and meter.

[8] Between 7 September and 13 October 2005, the generator was deployed at the Bermuda Institute for Ocean Science (BIOS) in a laboratory plumbed with local seawater. Seawater was pumped from a standpipe near the bottom (about 5 m below mean sea level) center of Ferry Reach (a well-flushed passage adjacent to the station) to a 9.6 m^3 fiberglass reservoir and fed via gravity into the laboratory; all pipes were PVA. The average turnover time for water in the reservoir was approximately 30 min. Most of the plumbing had been in continuous use for approximately

Table 1. Generator Characteristics Under Typical Set of Operating Conditions

Characteristic	Value
Diameter, cm	20
Cross section, cm^2	314
''Ocean'' depth, cm	133
''Ocean'' volume, L	42
''Ocean'' water turnover rate,[a] L min^{-1}	4.0
''Ocean'' water residence time,[a] min	10
''Ocean'' water upwelling velocity,[a] cm min^{-1}	13
Average bubble rise distance, cm	115
Bubbling rate,[a] L min^{-1}	5.0
Average bubble diameter,[b] μm	400
Average bubble rise velocity,[a] cm min^{-1}	627
Average bubble air residence time,[a] min	0.18
''Atmosphere'' depth, cm	81
''Atmosphere'' volume, L	26
''Atmosphere'' sweep air,[a] L min^{-1}	35
Upper ''atmosphere'' turnover rate,[a,c] L min^{-1}	40
Lower ''atmosphere'' upwelling velocity,[a,c] cm min^{-1}	16
Upper ''atmosphere'' upwelling velocity,[a,c] cm min^{-1}	127
Lower ''atmosphere'' residence time,[a,c] min	1.5
Upper ''atmosphere'' residence time,[a,c] min	0.45

[a]Variable parameter.
[b]Within several cm below the air-water interface.
[c]''Upper'' and ''lower'' refer to above and below the sweep-air injection ports, respectively, at 24 cm above air-water interface.

30 years and, thus, was well leached. The centrifugal pump was configured with a noncorrosive, graphite (Carbate) impellor and housing that had been in continuous service for about 3 years. As described in more detail below, chemical analyses indicated that seawater entering the generator was reasonably representative of the oligotrophic Sargasso Sea. Additional information concerning the characteristics of surface seawater in this region is available through the Web site for the Bermuda Atlantic Time Series at http://www.bbsr.edu/cintoo/bats/bats.html.

[9] In addition to the standard configuration described above, the generator was operated briefly in two other configurations. During the preliminary setup, the generator was filled and operated with DIW. The corresponding bubbles were much larger than those formed during subsequent operation with seawater. These differences in bubble size reflect the substantially lower surface tension of seawater relative to pure water. The system was also operated briefly with seawater flowing in the opposite direction (from top to bottom). This configuration resulted in the gradual but continual accumulation (over several hours) of surfactant material at the interface, which eventually capped the surface with a thick foam layer that attenuated aerosol production. Apparently, surfactant material was delivered to the surface by rising bubbles faster than it was emitted across the interface by bursting bubbles thereby leading to the observed accumulation. Reversing the flow (i.e., seawater flowing from bottom to top) constantly refreshed the surface and prevented the accumulation of surfactant material at the interface; no foam layer was noted under this latter set of conditions.

[10] After the preliminary setup, the generator was operated in three basic configurations. During the initial phase of the experiment, the generator's performance was characterized over ranges in bubble, sweep, and seawater flow rates and in RH based on aerosol number size distributions measured with an Aerodynamic Particle Sizer (APS, TSI Model 3310) sampling at 5.0 L min^{-1} and with a Scanning Mobility Particle Sizer (SMPS, TSI Model 3934L) sampling at 3.3 L min^{-1}. Airflow rates in the APS were calibrated and, if necessary, adjusted daily with a Gilibrator® Primary Standard Airflow Calibrator. Airflow rates in the SMPS were checked and, if necessary, adjusted at least 5 times per day using the mass flowmeters built into the instruments. Calibration of the SMPS mass-flowmeters was checked every 3 to 5 days using a Gilibrator®. The SMPS was configured such that filtered sample air was used for sheath air. A Vaisala Humicap temperature/relative humidity probe was mounted in a fitting to measure the exhaust of the electrostatic classifier not directed to the condensation particle counter. Since the SMPS was deployed immediately adjacent to the aerosol generator in a temperature-controlled laboratory, the temperature and RH of the air inside the electrostatic classifier matched that of the air exiting the sea-salt-aerosol generator.

[11] The APS and SMPS continuously characterized number size distributions from 0.013-μm to >15-μm diameter; the integration time for each set of observations was 5 min and the overlap between the two instruments was about 0.70 to 0.80 μm. About 30 min were required between each set of observations to adjust operating conditions and allow aerosol generation to reach steady state. Reported performance characteristics correspond to individual number size distributions averaged over 20 to 30 min of operation thereafter. Time constraints precluded chemical characterization of aerosols corresponding to each set of conditions during this initial phase of the experiment. The generator was blank tested by turning off and draining the seawater, maintaining the flow of sweep and bubble air, and sampling the exhaust with the APS and SMPS. The instruments detected less than 1 particle per cm^{-3} indicating that production via bursting bubbles was the only significant source of aerosols in the generator under normal operating conditions.

[12] During the second phase of the experiment, size-resolved aerosols at an average RH of 79 ± 1.3% were sampled for chemical characterization using two, 8-stage (10 size fractions), nonrotating MultiOriface Uniform Deposit Impactors (MOUDIs) operating in parallel at 30 L min^{-1} each [*Marple et al.*, 1991; *Howell et al.*, 1998]. The 50% aerodynamic cutoff diameters for the inlet and each impaction stage were 18, 10, 5.6, 3.2, 1.8, 1.0, 0.56, 0.32, and 0.18 μm. One impactor was configured for analysis of major ionic constituents and the other for either soluble organic carbon (OC) or total Br. The APS and SMPS were operated concurrently during some impactor sampling periods. The latter phase of the deployment was devoted primarily to generating aerosol for chemical manipulation experiments over ranges of light and acidity [*Davis et al.*, 2006; Zhou et al., unpublished manuscript, 2007]. During this period, bulk aerosol was sampled at 30 L min^{-1} on 90-mm-diameter Teflon filters (Gelman 2-μm pore size) mounted in Teflon housings; the APS was operated concurrently during bulk sampling but the SMPS was not. Individual size-resolved and bulk samples for chemical analysis were typically collected over nominal 12- and 24-hour periods, respectively.

[13] The MOUDIs and bulk samplers were rinsed with DIW between uses and dried, loaded, and unloaded in a class-100 clean bench equipped with an upstream prefilter of activated charcoal and permanganate (D Mark OGBCC-02-375-03) to remove reactive trace gases from the feed air. The MOUDI for analysis of major ions was configured with 47-mm-diameter polycarbonate impaction substrates (Whatman 111107) and 37-mm-diameter quartz fiber backup filters (Pallflex 2500 QAT-UP). Exposed samples were transferred to precleaned 10-ml centrifuge tubes, immediately frozen, and transported to the University of Virginia (UVA). Samples were subsequently extracted by alternating cycling of vigorous shaking and vortexing in 5 ml DIW and analyzed for $HCOO^-$, CH_3COO^-, $(COO)_2^{2-}$, $CH_3SO_3^-$, SO_4^{2-}, Cl^-, Br^-, NO_3^-, NH_4^+, Na^+, K^+, Mg^{2+}, and Ca^{2+} by ion chromatography [*Keene et al.*, 2004].

[14] During most periods, the MOUDI for OC was configured with precombusted 47-mm-diameter aluminum impaction substrates (MOUDI MDI-247) and precombusted 37-mm-diameter quartz backup filters (Pallflex 2500 QAT-UP) for analysis of OC. Exposed samples were transferred to precombusted 10-ml Pyrex centrifuge tubes and extracted immediately in 5 ml of DIW via vigorous alternating cycles of shaking and vortexing over about 5 min each. Following extraction, most samples were analyzed on site using a Shimadzu Model TOC-V CSH high-temperature-combustion organic carbon analyzer. A few samples were

frozen, transported to SUNY Syracuse and analyzed with the same instrument after the deployment.

[15] During two sampling periods, the paired MOUDI was configured with Whatman-41 impaction substrates and backup filter for analysis of total (organic plus inorganic) particulate Br and the associated sea-salt tracers Mg and Na. Exposed substrates and final filters were transferred to precleaned (via repeated rinses with DIW) 10-ml centrifuge tubes, immediately frozen, and transported to Mount Washington Observatory for processing. These samples were spiked with 20 ng In as an internal neutron flux monitor and subsequently analyzed by neutron activation analysis (NAA) at the Rhode Island Nuclear Science Center using procedures similar to those described by *Keene et al.* [2007].

[16] Teflon filters used for bulk sampling were thoroughly rinsed with DIW and individually blanked before each use. Exposed samples were extracted sequentially into 3 separate 5-ml aliquots of DIW via alternating cycles of vigorous shaking and vortexing totaling about 10 min for each aliquot. The two extracted aliquots were combined in a Teflon beaker and then subdivided for analysis and manipulation experiments. Two mls of each bulk sample were transferred to a precleaned Pyrex tube, frozen, transported to UVA, and analyzed for the suite of ionic constituents listed above. One ml of each bulk sample was transferred to a precleaned glass vial and analyzed on site for OC. The efficiency of the extraction procedure for bulk samples was verified by analyzing a fourth extract from several exposed filters; analytes were below detection limits indicating quantitative recovery of soluble constituents. All data were corrected on the basis of dynamic handling blanks that were generated routinely and processed using procedures identical to those for samples.

[17] Feed seawater was sampled daily and analyzed for major ionic constituents and OC using procedures similar to those described above. For ionic analyses, seawater was diluted 1 to 250 with DIW into the analytical ranges for aerosol extracts and analyzed simultaneously using the same sets of standard solutions and audit materials. This procedure minimized the potential for systematic variability between seawater and aerosol compositions that could have resulted from separate analytical runs, different analytical ranges, and/or different sets of calibration solutions.

[18] Measurement precisions and detection limits (DLs) were estimated following *Keene et al.* [1989]. Analytical resolution for different sea-salt reference species varied among the sampling media (Teflon, polycarbonate, quartz fiber, and Whatman 41) and associated analytical techniques (IC and NAA). For samples collected on Teflon and polycarbonate media and analyzed by IC, Mg^{2+} provided the greatest resolution. Consequently, for all bulk samples (N = 21) and for all impactor substrates analyzed by IC (N = 63), enrichment factors relative to sea salt (EFs) were calculated on the basis of the ratio of the constituent of interest to Mg^{2+} measured in the sample divided by the corresponding median ratio of the constituent of interest to Mg^{2+} measured in seawater [e.g., *Sander et al.*, 2003].

[19] Low loadings coupled with high DLs for Mg^{2+} (and most other inorganic constituents) on the final quartz filters of the impactor samples analyzed by IC (N = 7) limited resolution of EFs for ionic species and OC associated with the smallest aerosol size fraction (geometric mean diameter, GMD = 0.13 μm). For this size fraction, SO_4^{2-} was present at the highest concentrations (median value = 0.099 nmol m^{-3}; range 0.054 to 0.162 nmol m^{-3}) relative to the estimated DL (0.078 nmol m^{-3}). On the basis of the assumption that SO_4^{2-} was conservative with respect to inorganic sea salt during aerosol production (discussed below), EFs and total sea-salt mass for the smallest size fraction were calculated using SO_4^{2-} as the sea-salt reference species.

[20] Total Na sampled on Whatman 41 medium and analyzed by NAA was above DLs in all size fractions whereas total Mg was below DLs in 7 of 20 size fractions. Consequently EFs for total bromine were calculated using total Na as the sea-salt tracer.

[21] Dry sea-salt volume was calculated on the basis of the density of NaCl (2.165 g cm^{-3}). Organic mass was estimated by multiplying OC by a factor of 2 to account for the associated H and O [*Turpin and Lim*, 2001]. Dry organic volume was estimated on the basis of an assumed density of 1.1 g cm^{-3} [*Schkolnik et al.*, 2006].

3. Results and Discussion

3.1. Chemical Composition of Feed Seawater

[22] The ionic compositions of seawater sampled sequentially (over a period of about 10 min) several cm below the nearshore surface of Ferry Reach, below the surface within the reservoir for the gravity-feed seawater system, and at the feed port to the generator were statistically indistinguishable indicating no detectable influences from the pump and plumbing. The median concentration of Mg^{2+} measured in feed seawater (Table 2 and Figure 2) was 6% greater than the average for the surface ocean (53.1 mM [*Wilson*, 1975]). Variability in the ionic strength of feedwater as indicated by variability in Mg^{2+} reflects the combined influences of both analytical precision (±3%) and local effects due to dilution (e.g., from precipitation) and concentration (e.g., from evaporation). Median EFs for inorganic constituents in feedwater relative to average values for open-ocean water were within ±2% of 1.00 (Figure 2); the median EF for OC, which is inherently more variable, indicates enrichment of about 4% (Figure 2) relative to the annual average for the upper 200 m at the offshore Bermuda Atlantic Time Series Station (~0.064 mM C [*Carlson et al.*, 1994]). Concentrations of $HCOO^-$, CH_3COO^-, $(COO)_2^{2-}$, $CH_3SO_3^-$, NO_3^-, and NH_4^+ in feed seawater were all below analytical detection limits. These results indicated that the absolute and relative composition of feed seawater flowing through the generator was reasonably representative of the surrounding surface ocean.

3.2. Aerosol Physical Characteristics

[23] Important goals of this project included (1) evaluating the representativeness of the generated aerosols via characterization of physical and chemical properties and (2) maximizing production of representative aerosols for subsequent photochemical manipulation experiments. To achieve these goals, aerosol number size distributions and associate production fluxes were quantified as functions of basic controlling parameters including flow rates of bubble air, sweep air, and seawater.

Table 2. Summary Statistics for the Ionic and OC Composition of Feed Seawater and Nascent Aerosols[a]

GMD, μm	Statistic	SO_4^{2-}	Cl^-	Br^-	Mg^{2+}	Ca^{2+}	Na^+	K^+	OC
				Seawater, mM					
n/a	maximum	30.9	601	0.923	61.1	12.6	531	14.0	0.155
n/a	medium	29.6	572	0.883	56.1	10.9	504	11.0	0.0657
n/a	minimum	23.6	339	0.519	33.3	6.41	314	6.37	0.0445
n/a	average	28.9	535	0.825	52.8	10.4	474	10.8	0.0752
				Bulk Aerosol, nmol m^{-3}					
n/a	maximum	80.2	1519	2.36	144	34.7	1327	27.9	175
n/a	medium	53.3	1058	1.64	96.0	22.5	921	18.3	34.1
n/a	minimum	17.8	331	0.503	28.5	8.26	292	5.98	13.9
n/a	average	51.5	1002	1.55	94.6	22.1	881	17.5	54.8
				Size-Resolved Aerosol, nmol m^{-3}					
25.5	maximum	0.222	3.15	0.014	0.432	1.00	7.51	0.15	7.57
25.5	medium	0.138	2.32	0.006	0.245	0.10	3.89	0.07	3.72
25.5	minimum	0.094	1.32	0.002	0.199	<0.10	2.47	0.04	1.83
25.5	average	0.150	2.26	0.007	0.269	0.37	4.79	0.08	4.37
13.4	maximum	1.65	31.4	0.049	3.21	1.92	30.6	0.62	6.94
13.4	medium	1.24	23.4	0.041	2.39	0.77	26.6	0.57	5.01
13.4	minimum	0.941	18.1	0.030	1.58	0.51	24.9	0.32	1.15
13.4	average	1.32	25.3	0.041	2.39	1.05	27.7	0.51	4.43
7.48	maximum	10.4	173	0.283	22.2	6.35	166	3.48	8.59
7.48	medium	7.82	144	0.224	16.4	6.12	135	2.69	2.15
7.48	minimum	6.68	126	0.196	14.7	3.32	117	2.36	<1.15
7.48	average	8.32	145	0.231	17.5	5.36	139	2.84	3.53
4.23	maximum	17.1	253	0.429	38.4	8.91	235	4.45	12.9
4.23	medium	10.1	162	0.262	24.6	7.06	157	2.71	4.50
4.23	minimum	5.03	85.2	0.138	10.1	2.93	80.3	1.58	1.41
4.23	average	10.9	166	0.275	23.9	6.67	155	2.91	6.76
2.40	maximum	6.56	103	0.178	16.4	3.91	99.7	1.90	11.1
2.40	medium	3.52	57.0	0.092	8.51	2.95	61.8	1.12	8.22
2.40	minimum	1.75	33.1	0.052	3.56	1.04	32.7	0.66	3.56
2.40	average	4.03	64.3	0.107	8.96	2.79	63.1	1.18	7.26
1.34	maximum	3.52	55.4	0.092	8.97	2.53	55.3	1.03	9.72
1.34	medium	2.10	33.2	0.057	4.84	2.17	36.5	0.63	6.06
1.34	minimum	1.26	22.6	0.036	2.57	0.78	22.5	0.43	4.92
1.34	average	2.36	37.0	0.061	5.15	1.83	37.3	0.67	7.22
0.75	maximum	0.693	11.6	0.021	1.44	1.68	14.2	0.32	10.2
0.75	medium	0.543	9.09	0.019	0.902	0.62	10.6	0.18	5.78
0.75	minimum	0.344	6.91	0.010	0.674	0.25	7.42	0.14	4.64
0.75	average	0.557	9.62	0.017	0.994	0.73	10.9	0.21	6.98
0.42	maximum	0.556	6.93	0.013	0.673	0.93	11.6	0.22	9.66
0.42	medium	0.285	5.08	0.012	0.460	0.25	6.64	0.12	7.29
0.42	minimum	0.136	2.68	0.005	0.268	<0.10	3.37	<0.10	5.59
0.42	average	0.307	5.10	0.011	0.466	0.31	6.99	0.13	7.62
0.24	maximum	0.413	5.04	0.011	0.495	0.73	9.06	0.24	9.26
0.24	medium	0.208	4.00	0.010	0.336	0.20	4.97	0.12	7.05
0.24	minimum	0.088	1.80	0.002	0.174	<0.10	2.53	<0.10	4.49
0.24	average	0.222	3.69	0.008	0.348	0.29	5.33	0.14	7.28
0.13	maximum	0.162	<21	0.012	<0.16	0.11	<15	0.44	27.0
0.13	medium	0.099	<21	0.003	<0.16	0.05	<15	<0.19	19.7
0.13	minimum	0.054[b]	<21	<0.001	<0.16	<0.02	<15	<0.19	7.24
0.13	average	0.098	<21	0.005	<0.16	0.05	<15	<0.19	18.0

[a]The numbers of individual measurements (Ns) represented by the sample statistics for seawater are 24 for inorganic species and 16 for OC; for bulk aerosols, Ns are 19 for inorganic species and 18 for OC; and for size-resolved aerosols with paired inorganic and OC data, Ns are 5 for all analytes in each size fraction.

[b]Marginally less than the detection limit (0.078 nmol SO_4^{2-} m^{-3}); this value was the best estimate of inorganic sea salt associated with that sample and, thus, was used to calculate corresponding EFs; see text.

[24] Two factors constrained interpretation of the resulting data. The design of the generator precluded explicit differentiation of the primary production of aerosols from bursting bubbles at the interface and their subsequent entrainment into the sample-air stream. Sweep air entered the generator 24 cm above the interface (Table 1). Variability in bubble rates (1 to 5 L min^{-1}) resulted in corresponding variability in average upwelling velocities (3 to 16 cm min^{-1}, respectively) and average residence times (7.5 to 1.5 min, respectively) of air in the lower 24 cm of the model atmosphere. Consequently, some segregation as functions of both size and initial droplet injection height may have occurred over the range in bubble rates. Hereafter, the term production refers to the combined influences of both primary aerosol production and entrainment.

[25] In addition, flow rates of sweep air were dictated in part by the combined airflow required for sampling systems. For paired MOUDI samples, the sweep plus bubble airflow was 73 to 78 L min^{-1} whereas for bulk samples it was 40 L min^{-1}. Because the vertical velocity of air within the upper model atmosphere was greater during impactor relative to bulk sampling (about 238 versus 127 cm min^{-1}, respectively), the corresponding size distribution of aerosols would have shifted slightly toward larger particles. However, at a given bubble rate, the aerosol number production flux did not vary systematically as a function of total (sweep plus bubble) airflow (see below), which implies that this effect was small compared to other sources of variability in aerosol production.

3.2.1. Number Production Flux Versus Bubble Rate

[26] For a given set of conditions, the absolute number production fluxes increased with increasing bubble rate, although the relative size distributions of the fluxes were similar at all bubble rates (Figure 3). At 82% RH, maxima in the number production fluxes at all bubble rates were associated with particles about 0.13 μm diameter. At bubble rates less than or equal to 7 L min^{-1}, seawater feed rates less than or equal to 5 L min^{-1}, and constant RH (81 ± 2%), the number production fluxes of both super- and sub-μm-diameter size fractions exhibited significant linear correlations with bubble rate (Figure 4). At higher bubble or seawater flow rates, production fluxes, particularly for the larger size fractions, diverged from linearity with proportionately fewer particles produced. Visual inspection indicated that at the higher bubble and seawater flow rates, a thick (several mm) continuous bubble raft formed at the air-water interface, which we infer attenuated injection of fresh aerosols across the interface. This characteristic of the system imposed an effective upper limit on rates of aerosol production. On the basis of these results, most samples collected subsequently for chemical analysis and manipulation were generated under a standard set of conditions corresponding to bubble rates of 5 L min^{-1} and seawater flow rates of 4 L min^{-1}.

[27] Results from two sets of chamber experiments [*Blanchard and Syzdek*, 1988; *Resch and Afeti*, 1992] indicate peak production of sub-μm aerosols in association with the bursting of relatively large bubbles (~2000-μm diameter); smaller bubbles in the size range near the water-air interface within our generator (200 to 600 μm diameter) yielded few sub-μm aerosols. If this curious relationship between bubble size and film-drop production is broadly representative of marine-aerosol production, it is possible that the smaller subsurface bubbles within our generator coalesced at the interface to form larger bubbles that subsequently burst and thereby sustained the efficient sub-μm aerosol production that we observed. Alternatively, other factors may lead to variability in relationships between

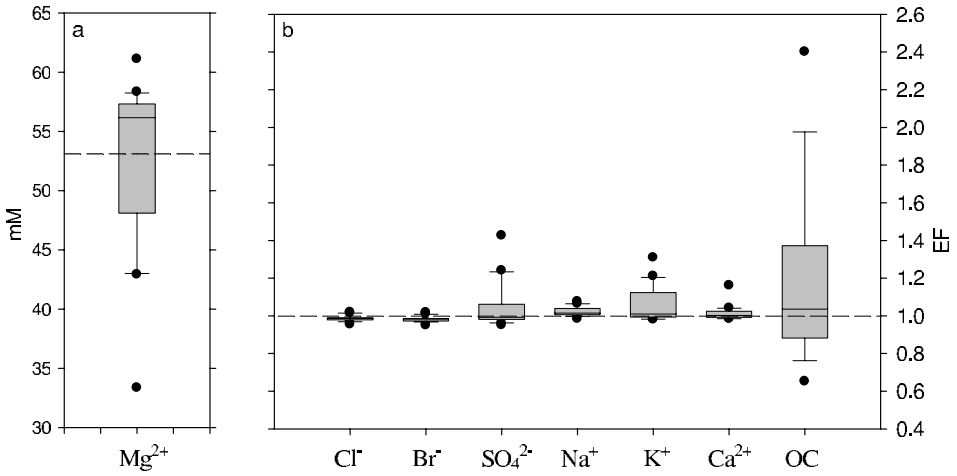

Figure 2. Distributions of (a) Mg^{2+} concentrations in feed seawater and (b) corresponding enrichment factors (EFs) for chemical constituents relative to the average composition of surface seawater using Mg^{2+} as the reference species. EFs for inorganic constituents (N = 24) are based on *Wilson* [1975]; those for OC (N = 16) are based on *Carlson et al.* [1994]. The horizontal line in Figure 2a depicts the average concentration of Mg^{2+} in surface seawater. Boxes and whiskers depict the 90th, 75th, median, 25th, and 10th percentiles; values outside this range are plotted individually.

bubble size and the corresponding size distribution of particles produced upon bursting. In this regard, we note that results from several other chamber studies do not indicate peaks in film drop production associated with ~2000 μm bubbles [e.g., see *Lewis and Schwartz*, 2004].

3.2.2. Number Concentration, Production Flux, and Water Content Versus RH

[28] At a constant bubble flow rate of 5.0 L min^{-1}, sweep plus bubble flow rate of 73 L min^{-1}, and seawater flow rate of 5 L min^{-1}, number concentrations of both super- and sub-μm size fractions (Figures 5 and 6) and the corresponding production fluxes (not shown but of identical shape) decreased systematically with decreasing RH between 95% and 50%. At RHs less than 50%, the number concentrations (Figure 6) and corresponding surface areas and volumes (not shown) exhibited little variability, which suggests that, in this RH range, the aerosols were almost completely dehydrated and thus insensitive to variable RH; marine-aerosol-hygroscopicity models predict similar behavior [*Gerber*, 1985; *Tang*, 1997]. The decrease in number concentrations of larger size particles with decreasing RH (Figure 6) is generally consistent with expectations based on hygroscopic properties; dehydration reduced some particles from greater than to less than 1.0-μm diameter. This effect is most evident between 95% and 80% RH. However, the essentially linear decrease in the number concentrations of sub-μm particles over this RH range was unexpected. These results suggest several possibilities: (1) Directional variability in aerosol production over the course of the measurements resulting from variability in the ionic strength or OC content of feed seawater (e.g., Figure 2), (2) the production of sub-μm aerosols decreased significantly as RH decreased from 95% and 50%, (3) dehydration to smaller size increased losses to surfaces, and/or (4) dehydration to smaller size increased losses due to coagulation.

[29] Unfortunately, variability in the composition of seawater was not characterized in parallel with these measurements so the potential influence of this factor on aerosol generation cannot be evaluated. We are aware of no mechanism by which the RH of the mixed layer would directly influence the corresponding number production flux from bursting bubbles. As is the case for the laminar sublayer overlying bulk seawater [e.g., *Lewis and Schwartz*, 2004],

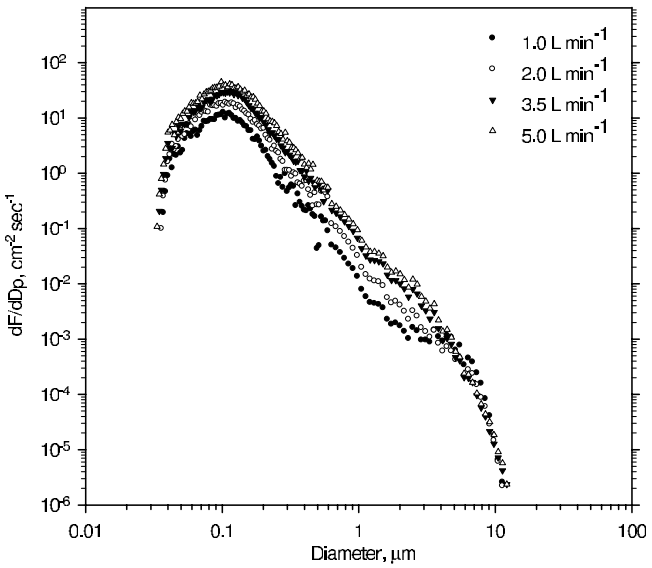

Figure 3. Size distribution of number production flux versus bubble rate at RH of 82 ± 1%; the flow rates for seawater and sweep plus bubble air were 5.0 and 73 L min^{-1}, respectively.

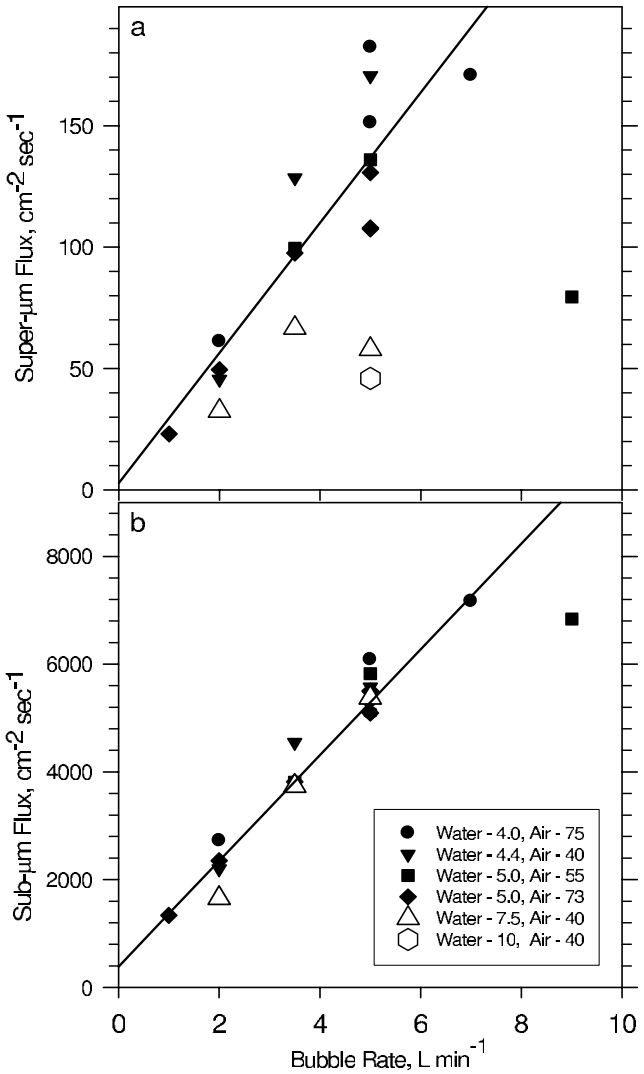

Figure 4. Total number production flux of (a) super-μm- and (b) sub-μm-diameter aerosols versus bubble rate at 81 ± 2% RH. In the legend, "water" refers to the seawater flow rate in L min^{-1} and "air" refers to combined sweep air plus bubble air flow rate in L min^{-1}. Lines depict standard linear regressions for all sets of observations (N = 18) corresponding to seawater flow rates less than or equal to 5 L min^{-1} (solid symbols) and bubble rates less than or equal to 7 L min^{-1} (see text). For Figure 4a, slope = 11.2 (cm^{-2} s^{-1}) (L min^{-1})$^{-1}$, Y intercept = −2.2 (cm^{-2} s^{-1}), and correlation coefficient = 0.85; for Figure 4b, slope = 968 (cm^{-2} s^{-1}) (L min^{-1})$^{-1}$, intercept = 514 (cm^{-2} s^{-1}), and correlation coefficient = 0.96. Data correspond to discrete sets of measurements over a 3-day period (14 through 16 September 2005).

the RH of the laminar sublayer overlying the bubble surface should be controlled primarily by the hygroscopic properties of the bubble surface itself not the RH of the mixed layer. In addition, while the RH of the mixed layer may influence the rate at which bubble caps thin, the burst itself should take place at about the same thickness independent of ambient RH.

[30] The measured size distributions (Figure 5) provide some insight concerning the likely underlying cause(s) for the observed variability. As RH decreased, the peak in sub-μm number concentration decreased from ~0.145-μm to ~0.080-μm diameter consistent with expectations based on water loss and the increasing shift toward very small particles (<0.08 μm diameter). This shift may have resulted in increased losses to surfaces and via coagulation between production and analysis. Because nascent particles produced by bursting bubbles are charged, electrostatic effects may be involved [e.g., *Blanchard*, 1963]. At lower RH, the static electrical relaxation time is relatively long compared to conditions at higher RH. The longer relaxation time coupled with smaller aerosol size at lower RH may have contributed

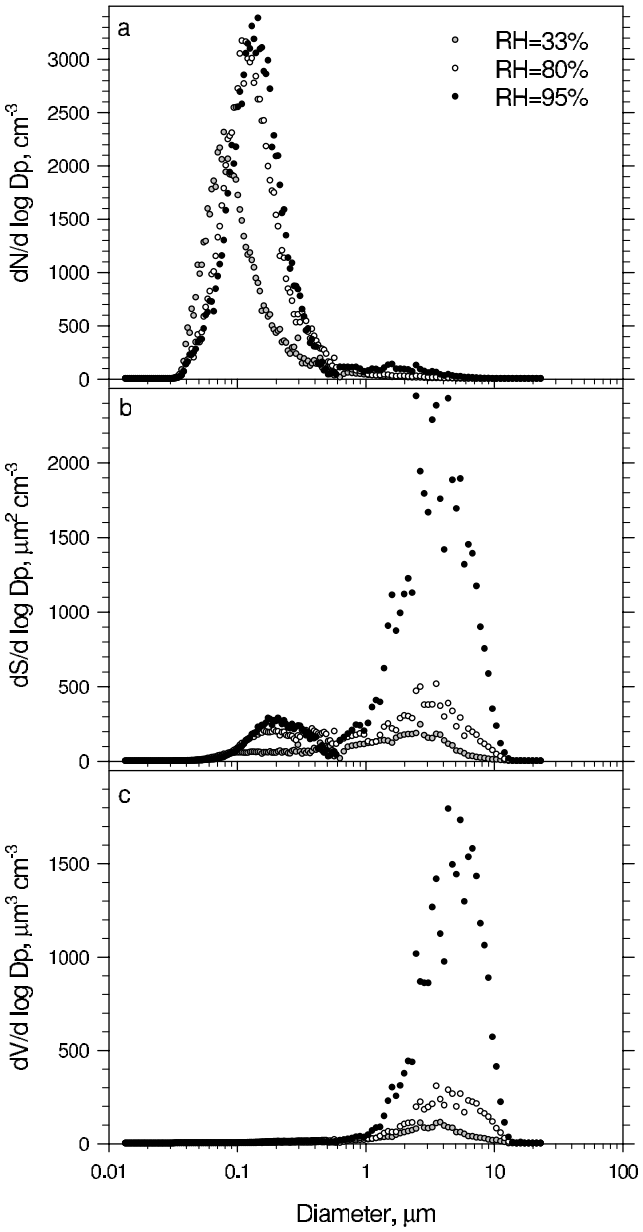

Figure 5. Aerosol (a) number, (b) surface area, and (c) volume size distributions at 33%, 80%, and 95% RH; the flow rates for seawater and sweep plus bubble air were 5.0 and 73 L min^{-1}, respectively.

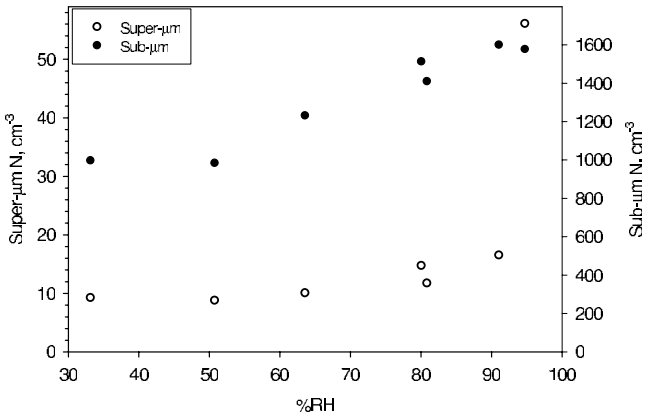

Figure 6. Total number concentrations of super-μm- and sub-μm-diameter aerosols versus RH.

to relatively greater losses to surfaces within the generator. Increasing losses of very small particles with decreasing RH would be consistent with the somewhat asymmetric shape of the lower end of the number size distribution at 33% RH (Figure 5a). In contrast, charged particles would repel one another, which coupled with the relatively short residence time of aerosols within the generator (Table 1), suggests that coagulation was probably not a primary driver.

[31] Assuming that increased losses to surfaces was the dominant process responsible for the observed decreases in number concentrations with decreasing RH and that the effect was restricted to the smallest particles, these losses would have had virtually no influence on the corresponding aerosol volume or mass flux. At 33% RH, the smallest 37% of the number distribution (diameters less than 0.079 μm) accounted for less than 1% of the corresponding sub-μm aerosol volume (i.e., volume integrated over all size bins less than 1-μm diameter). Consequently, for a given set of bubble, sweep, and seawater flow rates and seawater composition, the "dry" volumes and fluxes measured at RH less than ~50% would have been approximately equal to the corresponding volumes and mass fluxes of nonwater aerosol constituents at higher RHs. Thus, assuming that the aerosols at low RH were completely dehydrated, differences between "wet" volumes at higher RHs and the corresponding "dry" volumes at RHs less than 50% would have been approximately equal to the associated water volume. The observed volumes (Figure 5c) suggest that, for this set of conditions, water comprised approximately 53% and 59% of sub-μm aerosol volume at 80% and 95% RH, respectively. The corresponding water volumes of super-μm aerosols were 59% and 74%, respectively. These water contents are somewhat lower than those predicted by hygroscopicity models of marine aerosol [e.g., *Gerber*, 1985; *Tang*, 1997]. We return to this point below in the context of evaluating water content as a function of chemical composition.

3.3. Aerosol Chemical Characteristics

3.3.1. Major Ionic Constituents

[32] The relative size distributions of major inorganic constituents (Cl^-, SO_4^{2-}, Na^+, Mg^{2+}, K^+, Ca^{2+}; e.g., Table 2 and Figure 7) were similar to those measured over the open ocean at Bermuda [e.g., *Turekian et al.*, 2003] and elsewhere [*Pszenny et al.*, 2004]. Sea-salt mass typically peaked in the 4.2-μm-GMD-size fraction. Compared to the long-term annual average for near-surface air at Bermuda (e.g., 20.9 nmol Mg^{2+} m^{-3} based on *Galloway et al.* [1993]), the absolute inorganic concentrations (Table 2 and Figure 8) were generally greater by factors of 2 to 8, although the ranges in concentrations overlapped. With the exception of K^+ and Ca^{2+}, EFs for major ionic constituents (Figure 8) were statistically indistinguishable from 1.0 indicating no significant fractionation during aerosol production. Although the relatively small differences between

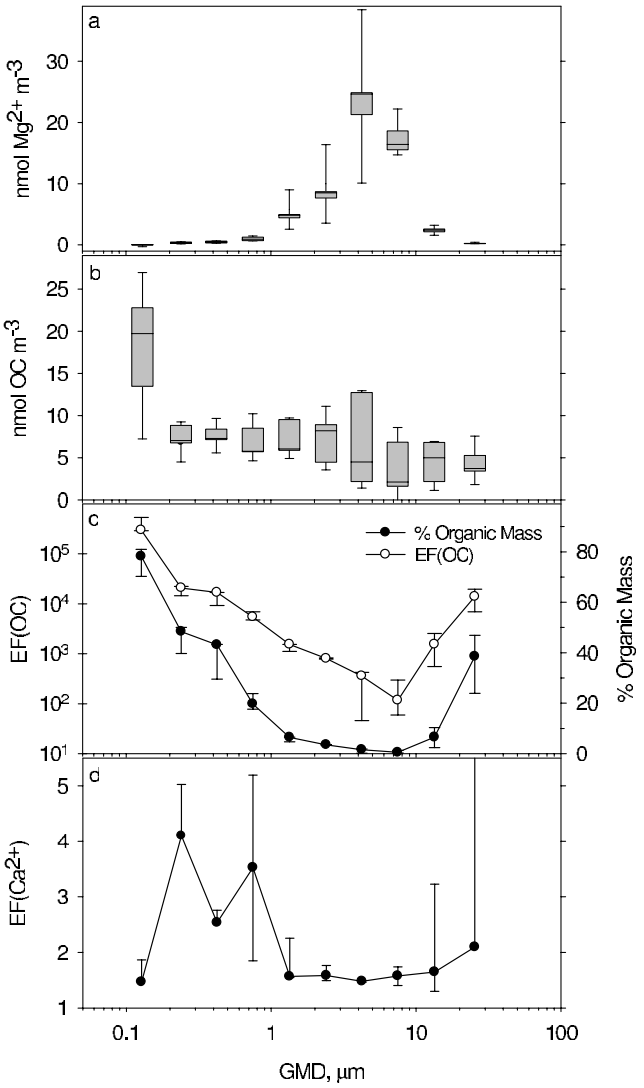

Figure 7. Box and whisker plots depicting maximum; 75th, median, and 25th percentiles; and minimum values for paired concentrations of size-resolved (a) Mg^{2+} and (b) OC (N = 5); corresponding median values for (c) EF(OC) and the percentage of organic to total (sea salt + organic) nonwater aerosol mass; and (d) median values for EF(Ca^{2+}). Error bars on Figures 7c and 7d correspond the 75th and 25th percentiles; percentiles corresponding to Ca^{2+} concentrations below DLs (for the largest and the three smallest size fractions) are not depicted.

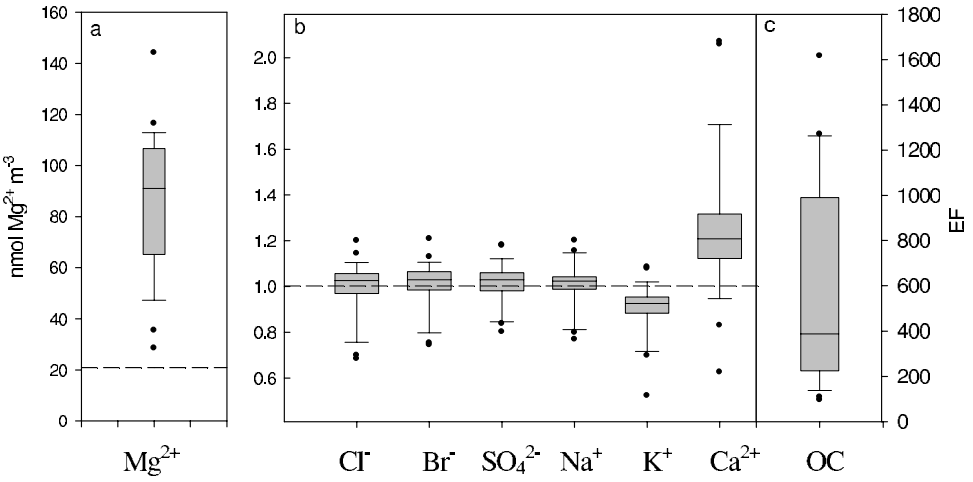

Figure 8. Distributions of (a) Mg^{2+} concentrations associated with nascent marine aerosols (N = 26) and corresponding EFs for (b) inorganic constituents (N = 26) and (c) OC (N = 23) relative to the median composition of feed seawater using Mg^{2+} as the reference species. Data correspond to 19 bulk samples (18 with both ionic and OC data and 1 with ionic data only) and 7 size-resolved samples (5 with ionic and OC data and 2 with ionic data only). Data for size-resolved samples are based on concentrations summed over all fractions. EFs for total Br (not shown, N = 2) were 1.07 and 1.09. The horizontal line in Figure 8a depicts the annual average concentration of particulate Mg^{2+} at Bermuda [*Galloway et al.*, 1993]. Boxes and whiskers depict the 90th, 75th, median, 25th, and 10th percentiles; values outside this range are plotted individually.

EFs for K^+ (Figure 8) and 1.0 were marginally significant, the overall agreement was within the absolute accuracy of the measurements. As with the feed seawater, concentrations of $HCOO^-$, CH_3COO^-, $(COO)_2^{2-}$, $CH_3SO_3^-$, NO_3^-, and NH_4^+ were below analytical detection limits in both size-fractioned and the bulk aerosol samples.

[33] The significant and systematic (24 of 26 samples) enrichment of Ca^{2+} relative to feed seawater (Figure 8) was unexpected. On the basis of the quality assurance information summarized above, it is unlikely that these enrichments resulted from some type of handling or analytical artifact. The nature of this apparent fractionation cannot be resolved unequivocally on the basis of our measurements but two processes may be involved. The enriched Ca^{2+} may have originated from fragments of biogenic $CaCO_3$ [e.g., *Sievering et al.*, 2004]. If so, this process would be an important source of alkalinity for marine aerosols that could have globally significant implications for aerosol pH and associated pH-dependent chemical processes. For example, assuming an equivalent ratio for HCO_3^- to Mg^{2+} in seawater of 0.0223 [e.g., *Keene et al.*, 1986] and no fractionation during aerosol production, the median concentration of Mg^{2+} measured during the experiment (91.0 nmol m^{-3}) would correspond to 4.1 neq HCO_3^- m^{-3}. By comparison, if the enriched Ca^{2+} were in the form of $CaCO_3$, the median EF for Ca^{2+} (Figure 8) would correspond to 7.8 neq CO_3^{2-} m^{-3} or almost twice the alkalinity associated with sea-salt HCO_3^-. Numerous studies have reported Ca^{2+} enrichments in marine aerosols and precipitation that are generally attributed to crustal dust transported from distant continents and/or locally produced wind-blown calcareous shell debris. Our results suggest that direct emission of $CaCO_3$ in association with the production of marine aerosols from bursting bubbles may also be a significant in situ source of alkalinity in marine air. Given its potential importance for acid-base chemistry in the marine boundary layer, the nature of this fractionation process, the speciation of the enriched Ca^{2+}, and the magnitude of the flux warrant further investigation.

[34] It is also possible that the Ca^{2+} was enriched in the aerosols through its complexation to organic matter. As discussed below, OC was highly enriched in the nascent aerosols (Figures 7c and 8) and the surface-active organic matter that absorbs to bubbles in seawater is highly sulfonated [*Zhou et al.*, 1998]. Consequently, this material could have significantly and selectively complexed Ca^{+2} (assuming higher stability constants with the organic matter relative to Mg^{+2}) thereby contributing to the observed enrichments. On average, the Ca^{2+} EFs were somewhat greater for the organic-rich sub-μm size fractions relative to the super-μm size fractions (Figures 7c and 7d) suggesting a possible direct link between the relative amount of organic matter and corresponding Ca^{2+}. However, about 95% inorganic sea salt was associated with super-μm size fractions and, consequently, summed over all size fractions, super-μm aerosols accounted for virtually all of the enriched Ca^{2+}. Note that if the excess Ca^{2+} were in the form of organic complexes, it would probably not provide additional alkalinity.

3.3.2. Particulate Bromine

[35] Under many conditions, sub-μm size fractions of ambient marine aerosols are highly enriched in Br relative to surface seawater but the processes responsible for these enrichments are not understood [e.g., *Sander et al.*, 2003]. One possible explanation involves enrichment of Br during aerosol formation. Ionic Br^- associated with artificially generated aerosol was present at ratios indistinguishable

from those in surface seawater (EFs ≈ 1.0, Figure 8), which indicates conservation during aerosol production from bursting bubbles. However, the corresponding OC is highly enriched (Figure 8). If the pool of enriched OC includes organic Br-containing compounds, this fractionation process may contribute to the unexplained Br enrichments observed in ambient sub-μm marine aerosols [e.g., *Sander et al.*, 2003].

[36] Total particulate Br, Na, and Mg were measured by NAA in two sets of impactor samples. On the basis of concentrations summed over all size fractions and using Na as the sea-salt reference species (see section 2), EF(Br)s for the two samples were 1.07 and 1.09, which were statistically indistinguishable from 1. For both samples, Br was undetectable in the final stage, which exhibited the greatest EF(OC)s (Figure 8). These results suggest that the large enrichments of Br that are often measured in sub-μm marine aerosol [e.g., *Sander et al.*, 2003] are not due to fractionation during aerosol production and, thereby, support the hypothesis that, over the remote open ocean, these enrichments originate primarily from multiphase chemical transformations in air.

3.3.3. Soluble Organic Carbon

[37] OC was highly enriched in all size-resolved and bulk aerosol samples (Figures 7 and 8). EF(OC)s generated during this experiment were similar in magnitude to those reported by *Hoffman* [1975] and *Hoffman and Duce* [1976] (range 130 to 640; average – 250; N = 11) using a bubbler-type apparatus deployed at Naragansett Bay, Rhode Island, USA. In contrast, EF(OC)s for ambient marine aerosols at Bermuda are substantially higher (average values of 1460 [*Hoffman and Duce*, 1977] and 6810 [*Turekian et al.*, 2003]).

[38] OC associated with the two largest aerosol size fractions were consistently enriched relative to the next smaller fractions (Figure 7c). Other laboratory studies of which we are aware do not resolve these larger size fractions. Given their relatively larger volumes, it is possible that particles in this size range incorporate disproportionately greater amounts of particulate organic material such as plankton, bacteria, and/or fragments thereof. They may also incorporate disproportionately greater amounts of organic material associated with the surface microlayer. Given the relatively short lifetimes of these larger aerosol size fractions (several hours), it is not expected that the observed enrichments in nascent aerosols would be reflected in size distributions in aged marine aerosols in ambient air.

[39] Because the atmospheric lifetimes of aerosols (and the associated OC) against deposition vary as a function of size, EF(OC)s for fresh artificially generated aerosols versus those for ambient aerosol sampled in bulk (or summed over impactor states) are not directly comparable. The mass-weighted atmospheric lifetimes of super-μm sea-salt dominated size fractions is on the order of 1.5 to 2 days whereas those for the sub-μm size fractions are on the order of 5 days [e.g., *Erickson et al.*, 1999]. On average, OC emitted in association with mechanically produced sub-μm aerosol will accumulate in the MBL to proportionately greater concentrations relative to that associated with the shorter-lived super-μm sea salt that is emitted in parallel. It follows that, in the absence of additional sources or sinks for primary, marine-derived OC, EF(OC)s in ambient marine air sampled in bulk would be substantially greater than the corresponding EF(OC)s for freshly emitted aerosols.

[40] On the basis of median values, sea salt dominated the mass of all but the smallest aerosol size fraction (Figure 7c). The GMD for the smallest size fraction sampled with the impactor (0.13-μm diameter) was approximately equal the number centroid for the sub-μm mode (Figure 5a), which indicates that organic constituents dominated the mass of most individual particles in this mode; sea salt was a minor component. The size distributions of laboratory generated aerosols reported by *Hoffman and Duce* [1977] do not reflect the large enrichments in the smallest size fraction observed in this study. However, the lower end of the size range reported by *Hoffman and Duce* [1977] extends only to an approximate diameter of 0.6 μm and, consequently, lacks adequate resolution to characterize EF(OC) associated with smaller size fractions of nascent aerosols.

[41] In addition to those mentioned above, several factors that have been reported to influence EF(OC) in artificially generated aerosols were not evaluated as part of this study. *Hoffman* [1975] and *Hoffman and Duce* [1976] examined the influence of bubble injection depth on EF(OC). On the basis of paired data (N = 5) the median EF(OC) at 104 cm (314) was 35% greater than that at 33 cm (203). The effect was nonlinear (e.g., delta EF(OC) decreased with increasing length), which suggests an asymptotic relationship. This result implies that EF(OC) in nascent ambient aerosols varies as a function of air injection depth and, thus, turbulence at the air-sea interface. As indicated above, field measurements of bubble clouds suggest that the average injection depth and associated lifetimes of bubbles within our generator were reasonably representative of the surface ocean.

[42] Bubble size and bubbling rate also influences EF(OC) for mechanically generated aerosols. Relative to larger bubbles, smaller bubbles are more effective in transporting surface-active organic compounds from artificial seawater solutions to the overlying air. In addition, the sea-to-air flux of organics is linearly correlated with bubble rate [*Tseng et al.*, 1992]. On the basis of visual inspection, most rising bubbles in our generator quickly (within about the first 30 cm) evolved into a fairly uniform size distribution; diameters near the water-air interface ranged from about 200 to 600 μm. Presumably, this behavior is related to the buoyant versus surface tension forces of the aqueous solution, which vary as a function of chemical composition [*Russell and Singh*, 2006]. On the basis of *Tseng et al.* [1992], we infer that the generally smaller, freshly emitted bubbles near the bottom of the water column scavenged surfactants more efficiently than did the relatively larger bubbles near the interface. As mentioned in section 2, time constraints precluded chemical analysis of aerosol samples during the initial, physical characterization phase of the experiment. Given that the number production fluxes of both super- and sub-μm size fractions were linearly correlated with bubble rate (Figure 4), we infer on the basis of *Tseng et al.* [1992] that the corresponding fluxes of organics were also linearly correlated with bubble rate.

[43] Other potentially important variables including temperature and the OC concentration (and presumably speciation, which was not measured) in the feed seawater varied over relatively narrow ranges (e.g., Figure 2). Consequently,

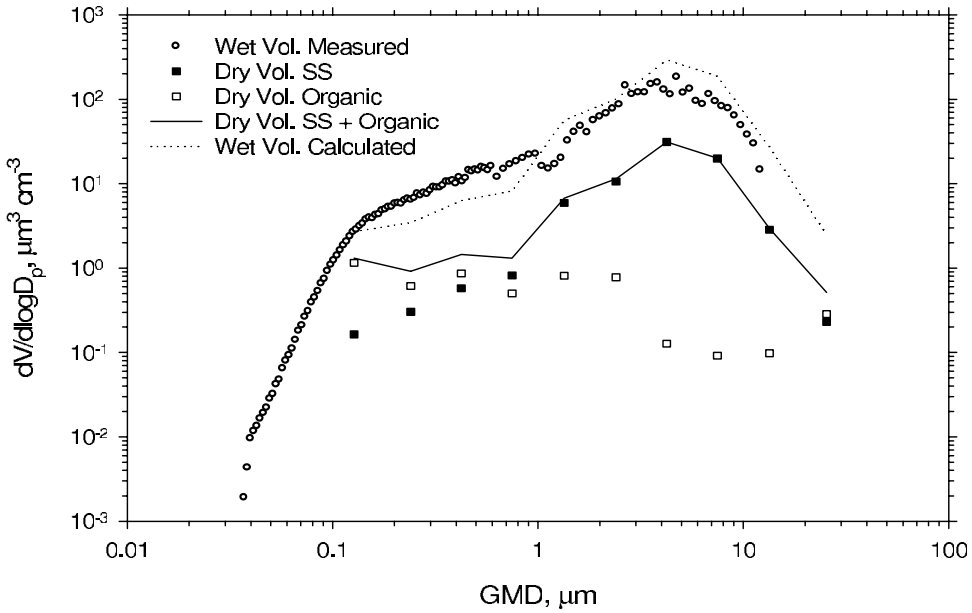

Figure 9. Comparison among size distributions of the average (N = 3) "wet" aerosol volume measured with the APS and SMPS at an RH of 77.6 ± 1.4 (open circles), the nonwater "dry" volume of sea salt (solid squares) and organic material (open squares), the sum of dry sea-salt and organic volume (solid line), and the corresponding "wet" aerosol volume based on the measured sea-salt concentration and the hygroscopic properties of NaCl [*Tang*, 1997] assuming no influence of organic material on water content.

we were unable to evaluate the associated influences of variability in these parameters on the corresponding number production fluxes and EF(OC)s for aerosols emitted by bursting bubbles.

3.3.4. Water Content as a Function of Chemical Composition

[44] During two sampling periods complete number size distributions were measured in parallel with size-resolved concentrations of inorganic ionic constituents and OC. These data allow explicit evaluation of aerosol water content as a function of chemical composition via two complimentary approaches. Water volume was inferred directly from differences between the size distributions of deliquesced aerosol volume measured with the APS and SMPS and the corresponding dry volumes based on the densities of measured sea salt and organic material. Total aerosol volumes were also calculated for a given RH on the basis of the measured sea-salt and organic concentrations and the associated hygroscopic properties of NaCl [*Tang*, 1997] on the basis of the assumption that organic species did not influence hygroscopicity. Within the resolution of the measurements, the two approaches yielded consistent estimates of aerosol water content (Figure 9 and Table 3). These results imply that water contents of nascent marine aerosols are controlled primarily by the hygroscopic properties of associated sea salt.

[45] These results also suggest that the differences between aerosol volumes measured with the APS and SMPS

Table 3. Summary Comparison of Aerosol Water Contents Inferred From Direct Measurements of Paired Physical and Chemical Properties Versus Those Calculated From Measured Sea-Salt and OC Concentrations, RH, and the Hygroscopic Properties of NaCl[a]

	Measured Wet Volume,[b] μm^3 cm^{-3}	Dry SS Mass, μg m^{-3}	Dry SS Volume, μm^3 cm^{-3}	Dry Organic Mass, μg m^{-3}	Dry Organic Volume, μm^3 cm^{-3}	Dry SS + Organic Volume, μm^3 cm^{-3}	Water Content,[c] % volume (From Data)	Water Content,[d] % volume [*Tang*, 1997]
16 September 2005 (RH = 77.6 ± 1.4)								
Super-μm diameter	87.1 ± 11.2	37.9 ± 2.1	17.5 ± 0.96	0.86 ± 0.029	0.78 ± 0.027	18.3 ± 0.96	79 ± 13	89.4
Sub-μm diameter	9.9 ± 6.5	1.00 ± 0.06	0.46 ± 0.03	0.59 ± 0.038	0.53 ± 0.035	1.0 ± 0.044	90 ± 65	88.7
Total	97.6 ± 10.6	39.0 ± 2.2	18.0 ± 1.00	1.45 ± 0.047	1.32 ± 0.043	19.3 ± 1.00	80 ± 11	89.4
18 September 2005 (RH = 80.9 ± 1.1)								
Super-μm diameter	204 ± 3.5	58.3 ± 3.2	26.9 ± 1.47	1.06 ± 0.027	0.97 ± 0.025	27.9 ± 1.47	86 ± 2	90.2
Sub-μm diameter	11.7 ± 2.9	1.89 ± 0.11	0.87 ± 0.05	0.69 ± 0.015	0.62 ± 0.014	1.5 ± 0.053	87 ± 24	90.1
Total	216 ± 3.5	60.2 ± 3.2	27.8 ± 1.50	1.75 ± 0.039	1.59 ± 0.035	29.4 ± 1.50	86 ± 2	90.2

[a]SS refers to sea salt.
[b]Size distributions (N = 3) were measured with the APS and SMPS at the specified RH within the generator over the nominal 12-hour sampling period corresponding to each set of chemical data. Volumes for each size distribution were integrated over the specified size range; reported values correspond to the average and standard deviation for each subset of volumes.
[c]Inferred from difference between wet and dry (sea salt + organic) volumes based on direct measurements.
[d]Calculated on the basis of the hygroscopic properties of NaCl [*Tang*, 1997].

at high versus low RHs (discussed above, section 3.2.2 and Figure 5) probably underestimated actual water contents. We infer that, at RHs near or below the crystallization RH for NaCl (about 48% at 25°C), the nascent aerosols lacked sufficient time to completely dehydrate into equilibrium during ~30-s exposure to sweep air. If aerosols at lower RH retained significant water, the difference approach would underestimate water content.

3.4. Implications

[46] Results of this investigation have important implications for our understanding of the multiphase chemical and physical evolution of the MBL and related influences on Earth systems including climate. Several empirical relationships have been developed and applied in models to predict the production of size-resolved marine aerosol as a function wind velocity or whitecap coverage [e.g., *Monahan et al.*, 1986; *Smith et al.*, 1993; *Andreas*, 1998; *Vignati et al.*, 2001; *Gong*, 2003; *Mårtensson et al.*, 2003; *Clarke et al.*, 2006]. Although the predicted fluxes of super-μm size fractions based on these relationships intercompare reasonably well, the earlier formulations either overpredicted [*Monahan et al.*, 1986] or underpredicted [*Smith et al.*, 1993] production of sub-μm aerosols substantially [*Andreas*, 1998; *Gong*, 2003]. Representative simulation of sub-μm aerosol production is essential to reliably evaluate associated influences on chemical processing, cloud microphysics, radiative transfer, and climate. *Vignati et al.* [2001] and *Gong* [2003] fit empirical corrections based on measured sea-salt size distributions reported by *O'Dowd et al.* [1997] to bring the production fluxes of sub-μm size fractions in line with those based on observations. However, the data for sub-μm aerosol from which these production functions were formulated are based on a thermal desorption technique that removes, as a function of temperature, volatile components (including OC) of ambient marine aerosols prior to physical characterization [*O'Dowd and Smith*, 1993; *O'Dowd et al.*, 1997]. The residual refractory component of sub-μm aerosol at ~600°C (primarily inorganic sea salt) is assumed to be representative of primary aerosol produced by bursting bubbles at the ocean surface. In addition, the lower limit for the size distributions reported by *O'Dowd et al.* [1997] (0.20 μm diameter at 80% RH) is substantially greater than the number centroid for the sub-μm size mode observed during this investigation (0.13 μm diameter at 80% RH, Figure 5a). To provide context, at all bubble rates, normalized production fluxes of aerosols within the generator for the size bin bracketing 0.13-μm diameter at 82% RH were a factor of about 3 times greater than those for the bin bracketing 0.20-μm diameter (Figure 3). Particles less than 0.20-μm diameter accounted for 76% (at a bubble rate of 5 L min^{-1}) to 83% (at a bubble rate of 1 L min^{-1}) of the total number production flux (Figure 3). We infer that the number size distributions of sub-μm marine aerosol reported by *O'Dowd et al.* [1997] were not representative of the original mixture of primary organic and inorganic constituents in freshly produced sub-um marine aerosols and, consequently, the formulations of *Vignati et al.* [2001] and *Gong* [2003] are probably not representative of the lower end of the size distribution.

[47] *Mårtensson et al.* [2003] measured size-resolved production fluxes of aerosols between 0.02 and 20 μm diameter that were generated by bubbling zero-air through artificial seawater over a range of water temperatures and salinities. The seawater was made from commercially available artificial sea salt of unreported and presumably unknown organic content dissolved in deionized water. Given the importance of organics evident in our results, it is difficult to evaluate the representativeness of these results.

[48] Recently, *Clarke et al.* [2006] reported concentrations and production fluxes of "dry" (at 40% RH) marine aerosols between 0.01 and 8 μm diameter based on vertical profiles of aerosol microphysical properties measured immediately downwind of breaking coastal waves. The experimental design is innovative but chemical characterization relies on thermal desorption (from 300° to 360°C) and the assumption that volatile organic material accounts for minor fractions of nascent aerosol mass, which our results suggest is probably not valid.

[49] The production functions developed by *Vignati et al.* [2001], *Gong* [2003], *Mårtensson et al.* [2003] and *Clarke et al.* [2006] have been implemented in several current 1-D and 3-D models [e.g., *Caffrey et al.*, 2006; *Mahowald et al.*, 2006; *Pierce and Adams*, 2006]. On the basis of the above, we infer that the abilities of these models to simulate relationships between primary marine aerosol production and cycling and the associated direct and indirect effects on the Earth's climate is constrained by incorrect underlying assumptions about the number size distributions and associated chemical characteristics of the nascent sub-μm marine particles.

[50] The studies cited above together with the results reported herein clearly indicate that the efficient production of primary, sub-μm, hygroscopic aerosols by bursting bubbles represents an important source of reactive media in marine air. At 80% RH, the associated surface area is approximately equal to that of super-μm size fractions (Figure 5b). As noted above, because of their longer atmospheric lifetime, sub-μm aerosols would accumulate to relatively higher concentrations in ambient air at steady state. In addition to efficiently scattering incident solar radiation and serving as CCN, primary sub-μm marine aerosols should, given their size and apparent hygroscopicity, facilitate multiphase transformations in marine air. For example, primary marine aerosols would compete with nuclear clusters (from gas-to-particle reactions) for condensable reaction products from gaseous precursors (e.g., H_2SO_4, CH_3SO_3H, and $(COOH)_2$) and thereby diminish the potential for clusters to grow into sustainable size. Although the incorporation of H_2SO_4 and other secondary products into primary marine aerosol would influence associated size and hygroscopic properties, it would not alter absolute number concentrations significantly [*Clarke et al.*, 2006]. Consequently, the influences of sulfur cycling in the MBL on aerosol production, light scattering, cloud microphysics, and climate may be substantially less than predicted on the basis of models that do not consider interactions involving the high number concentrations and associated surface area of primary aerosols produced at the ocean surface [*Pierce and Adams*, 2006].

[51] The observed ratios of Ca^{2+} to conservative sea-salt tracers suggest that alkalinity may be significantly enriched relative to bulk seawater during aerosol production. If so, for a given set of conditions, the S(IV) + O_3 reaction will be

much faster and significantly more S(VI) will be produced via this pathway relative to that predicted by most models [e.g., *Chameides and Stelson*, 1992; *Keene et al.*, 1998; *Erickson et al.*, 1999; *Pszenny et al.*, 2004]. In addition, aqueous phase chemical processes that are effectively limited to acidic conditions (e.g., halogen activation) would be relatively less important than predicted by most current models [e.g., see *von Glasow and Crutzen*, 2004]. To address this fundamental issue, it is essential that the speciation of the enriched Ca^{2+} be resolved.

[52] As discussed above and in the cited literature, OC associated with nascent marine aerosols is not conservative with respect to either the production of inorganic sea-salt constituents or subsequent physiochemical evolution. Consequently, it is very difficult to reliably estimate both production fluxes and associated characteristics of fresh sub-μm marine aerosols based on measurement in ambient air. We recognize the inherent limitations in extrapolating results of chamber experiments such as those reported herein to the ambient MBL. However, in light of current understanding and analytical capabilities, we view extrapolation (i.e., based on the major drivers including wind speed, fetch, whitecap coverage, and DOC concentration and speciation in surface seawater) as an essential approach for evaluating the importance of nascent marine aerosols on chemical processes in the MBL and related direct and indirect climatic influences.

4. Summary and Conclusions

[53] 1. The composition of feed seawater was reasonably representative of the surrounding surface ocean.

[54] 2. Relative size distributions of inorganic sea-salt constituents were similar to those measured in ambient air although, on average, the absolute concentrations were higher by factors of 2 to 8.

[55] 3. With the exception of Ca^{2+}, ionic species (including Br^-) and total Br in artificially generated aerosols were present at ratios indistinguishable from those in surface seawater.

[56] 4. Ca^{2+} was significantly enriched (median EF = 1.21). If in the form of $CaCO_3$, these enrichments would correspond to a large source of alkalinity (median factor of 2 greater than dissolved HCO_3^-) in marine aerosol with important implications for solution pH and associated pH-dependent processes including S oxidation and halogen activation.

[57] 5. OC was highly enriched in all aerosol size fractions (median EF for all samples = 387). Greatest enrichments were associated with the smallest size fraction (GMD = 0.13 μm).

[58] 6. Size distributions exhibited two discrete lognormal modes. The number production flux of each mode was linearly correlated with bubble rate. Number concentrations and apparent production fluxes decreased with decreasing RH; we hypothesize that decreasing aerosol size (from dehydration) coupled with longer static electrical relaxation times at lower RH led to relatively greater losses of smaller particles to surfaces within the generator.

[59] 7. At ~80% RH, the larger mode exhibited a volume centroid of ~5 μm and included ~95% of the inorganic sea-salt mass. Water comprised about 80% to 90% of the corresponding volume.

[60] 8. At ~80% RH, the smaller mode exhibited a number centroid of ~0.13 μm. Water comprised about 87% to 90% of the corresponding volume. The mass ratio of organic matter to sea salt in the smallest size fraction (GMD = 0.13 μm) was 4:1.

[61] 9. These results provide unequivocal confirmation that bursting bubbles at the ocean surface produce significant numbers of sub-μm, hygroscopic, organic-dominated aerosols and thereby support the hypothesis that this pathway is a potentially important global source of CN and CCN. These primary sub-μm aerosols would also scatter incident solar radiation and thereby influence radiative transfer directly.

[62] 10. With its large associated surface area, primary sub-μm aerosol would represent a potentially important reaction medium for multiphase chemical transformations in marine air.

[63] **Acknowledgments.** We thank R. von Glasow and the anonymous reviewer for helpful comments, the Bermuda Institute for Ocean Sciences for outstanding logistical support during the field deployments, and B. Deegan for performing neutron activation analyses. Financial support was provided by the U.S. National Science Foundation (NSF) through awards ATM-0343146 and ATM-0638741 to the University of Virginia, ATM-0343082 to the University of Miami, ATM-0343199 to SUNY Syracuse, and ATM-0343181 to Wadsworth Center. Additional support was provided by NSF through award ATM 0401622 to the University of New Hampshire (UNH), by the NOAA Office of Oceanic and Atmospheric Research through grants to UNH (NA04OAR4600154 and NA05OAR4601080), and by a Deutsche Forschungsgemeinschaft grant to the University of Heidelberg (GL 353-1/2). Any opinions, findings, and conclusions or recommendations expressed in this paper are those of the authors and do not necessarily reflect the views of NSF.

References

Anastasio, C., and J. T. Newberg (2007), Sources and sinks of hydroxyl radical in sea-salt particles, *J. Geophys. Res.*, *112*, D10306, doi:10.1029/2006JD008061.

Andreas, E. L. (1998), A new sea spray generation function for wind speeds up to 32 m s^{-1}, *J. Phys. Oceanogr.*, *28*, 2175–2184.

Bezdek, H. F., and A. F. Carlucci (1974), Concentration and removal of liquid microlayers from a seawater surface by bursting bubbles, *Limnol. Oceanogr.*, *19*, 126–132.

Blanchard, D. C. (1963), The electrification of the atmosphere by particles from bubbles in the sea, in *Progress in Oceanography*, edited by M. Sears, pp. 73–202, Elsevier, New York.

Blanchard, D. C. (1975), Bubble scavenging and the water-to-air transfer of organic material in the sea, *Adv. Chem. Series*, *145*, 360–387.

Blanchard, D. C., and L. D. Syzdek (1974), Importance of bubble scavenging in the water to air transfer of organic material and bacteria, *J. Rech. Atmos.*, *8*, 529–540.

Blanchard, D. C., and L. D. Syzdek (1988), Film drop production as a function of bubble size, *J. Geophys. Res.*, *93*, 3649–3654.

Blanchard, D. C., and A. H. Woodcock (1980), The production, concentration, and vertical distribution of the sea-salt aerosol, *Ann., N. Y. Acad. Sci.*, *338*, 330–347.

Caffrey, P. F., W. A. Hoppel, and J. J. Shi (2006), A one-dimensional sectional aerosol model integrated with mesoscale meteorological data to study marine boundary layer aerosol dynamics, *J. Geophys. Res.*, *111*, D24201, doi:10.1029/2006JD007237.

Carlson, C. A., H. W. Ducklow, and A. F. Michaels (1994), Annual flux of dissolved organic carbon from the euphotic zone in the northwestern Sargasso Sea, *Nature*, *371*, 405–408.

Chameides, W. L., and A. W. Stelson (1992), Aqueous-phase chemical processes in deliquescent sea-salt aerosols: A mechanism that couples the atmospheric cycles of S and sea salt, *J. Geophys. Res.*, *97*, 20,565–20,580.

Chesselet, R., M. Fontugne, P. Buat-Menard, U. Ezat, and C. E. Lambert (1981), The origin of particulate organic carbon in the marine atmosphere as indicated by its stable carbon isotopic composition, *Geophys. Res. Lett.*, *8*, 345–348.

Clarke, A. D., S. R. Owens, and J. Zhou (2006), An ultrafine sea-salt flux from breaking waves: Implications for CCN in the remote marine atmosphere, *J. Geophys. Res.*, *111*, D06202, doi:10.1029/2005JD006565.

Clift, R. J., R. Grace, and M. E. Weber (1977), *Bubbles, Drops and Particles*, Elsevier, New York.

Davis, A. J., E. Dahl, D. Kieber, X. Zhou, W. Keene, J. Maben, R. Sander, R. von Glasow, and L. Smoydzyn (2006), Photochemical production of oxidants in sea-salt aerosols, *Eos Trans. AGU*, *87*(52), Fall Meeting Suppl., Abstract A53A-017.

Decesari, S., M. C. Facchini, S. Fuzzi, G. B. McFiggans, H. Coe, and K. N. Bower (2005), The water-soluble organic component of size-segregated aerosol, cloud water and wet deposition from Jeju Island during ACE-Asia, *Atmos. Environ.*, *39*, 211–222.

Dickerson, R. R., K. P. Rhoads, T. P. Carsey, S. J. Oltmans, J. P. Burrows, and P. J. Crutzen (1999), Ozone in the remote marine boundary layer: A possible role for halogens, *J. Geophys. Res.*, *104*, 21,385–21,395.

Duce, R. A., and E. J. Hoffman (1976), Chemical fractionation at the air/sea interface, *Ann., Rev. Earth Planet, Sci.*, *4*, 187–228.

Erickson, D. J., C. Seuzaret, W. C. Keene, and S.-L. Gong (1999), A general circulation model calculation of HCl and $ClNO_2$ production from sea-salt dechlorination: Reactive chlorine emissions inventory, *J. Geophys. Res.*, *104*, 8347–8372.

Galbally, I. E., S. T. Bentley, and C. P. Meyer (2000), Mid-latitude marine boundary-layer ozone destruction at visible sunrise observed at Cape Grim, Tasmania, *Geophys. Res. Lett.*, *27*, 3841–3844.

Galloway, J. N., D. L. Savoie, W. C. Keene, and J. M. Prospero (1993), The temporal and spatial variability of scavenging ratios for nss sulfate, nitrate, methanesulfonate and sodium in the atmosphere over the North Atlantic Ocean, *Atmos. Environ., Part A*, *27*, 235–250.

Gerber, H. E. (1985), Relative-humidity parameterization of the Navy Aerosol Model (NAM), *NRL Rep. 8956*, Nav. Res. Lab., Washington, D. C.

Gershey, R. M. (1983), Characterization of seawater organic matter carried by bubble-generated aerosols, *Limnol. Oceanogr.*, *28*, 309–319.

Gong, S. L. (2003), A parameterization of sea-salt aerosol source function for sub- and super-micron particles, *Global Biogeochem. Cycles*, *17*(4), 1097, doi:10.1029/2003GB002079.

Hoffman, E. J. (1975), Chemical fractionation at the air sea interface: Alkali and alkaline earth metals and total organic carbon, Ph.D. dissertation, Univ. of Rhode Island, Providence, R. I.

Hoffman, E. J., and R. A. Duce (1976), Factors influencing the organic carbon content of marine aerosols: A laboratory study, *J. Geophys. Res.*, *81*, 3667–3670.

Hoffman, E. J., and R. A. Duce (1977), Organic carbon in atmospheric particulate matter: Concentration and particle size distribution, *Geophys. Res. Lett.*, *4*, 449–452.

Howell, S., A. A. P. Pszenny, P. Quinn, and B. Huebert (1998), A field intercomparison of three cascade impactors, *Aerosol Sci. Technol.*, *29*, 475–492.

Hunter, K. A. (1997), Chemistry of the sea-surface microlayer, in *The Sea Surface and Global Change*, edited by P. S. Liss and R. A. Duce, pp. 287–319, Cambridge Univ. Press, New York.

Intergovernmental Panel on Climate Change (2001), *Climate Change 2001: The Scientific Basis: Contribution of Working Group I to the Third Assessment Report of the Intergovernmental Panel on Climate Change*, edited by J. T. Houghton et al., 881 pp., Cambridge Univ. Press, New York.

Keene, W. C., A. A. P. Pszenny, J. N. Galloway, and M. E. Hawley (1986), Sea-salt corrections and interpretation of constituent ratios in marine precipitation, *J. Geophys. Res.*, *91*, 6647–6658.

Keene, W. C., et al. (1989), An intercomparison of measurement systems for vapor- and particulate-phase concentrations of formic and acetic acids, *J. Geophys. Res.*, *94*, 6457–6471.

Keene, W. C., D. J. Jacob, and S.-M. Fan (1996), Reactive chlorine: A potential sink for dimethylsulfide and hydrocarbons in the marine boundary layer, *Atmos. Environ.*, *30*(6), i–iii.

Keene, W. C., R. Sander, A. A. P. Pszenny, R. Vogt, P. J. Crutzen, and J. N. Galloway (1998), Aerosol pH in the marine boundary layer: A review and model evaluation, *J. Aerosol Sci.*, *29*, 339–356.

Keene, W. C., A. A. P. Pszenny, J. R. Maben, E. Stevenson, and A. Wall (2004), Closure evaluation of size-resolved aerosol pH in the New England coastal atmosphere during summer, *J. Geophys. Res.*, *109*, D23S07, doi:10.1029/2004JD004801.

Keene, W. C., J. Stutz, A. A. P. Pszenny, J. R. Maben, E. V. Fischer, A. M. Smith, R. von Glasow, S. Pechtl, B. C. Sive, and R. K. Varner (2007), Inorganic chlorine and bromine in coastal New England air during summer, *J. Geophys. Res.*, *112*, D10S12, doi:10.1029/2006JD007689.

Leck, C., and E. K. Bigg (2005), Source and evolution of the marine aerosol: A new perspective, *Geophys. Res. Lett.*, *32*, L19803, doi:10.1029/2005GL023651.

Lewis, E. R., and S. E. Schwartz (2004), *Sea Salt Aerosol Production: Mechanisms, Methods, Measurements, and Models-A Critical Review*, *Geophys. Monogr. Ser.*, vol. 152, AGU, Washington, D. C.

Lohmann, U., and C. Leck (2005), Importance of submicron surface active organic aerosols for pristine Arctic clouds, *Tellus, Ser. B*, *57*, 261–268.

Mahowald, N. M., J. F. Lamarque, X. X. Tie, and E. Wolff (2006), Sea-salt aerosol response to climate change: Last Glacial Maximum, preindustrial, and doubled carbon dioxide climates, *J. Geophys. Res.*, *111*(D5), D05303, doi:10.1029/2005JD006459.

Marple, V. A., K. L. Rubow, and S. M. Behm (1991), A Microorifice Uniform Deposit Impactor (MOUDI): Description, calibration, and use, *Aerosol Sci. Technol.*, *14*, 434–446.

Mårtensson, E. M., E. D. Nilsson, G. de Leeuw, L. H. Cohen, and H.-C. Hansson (2003), Laboratory simulations and parameterization of the primary marine aerosol production, *J. Geophys. Res.*, *108*(D9), 4297, doi:10.1029/2002JD002263.

McDow, S. R., M. Jang, Y. Hong, and R. M. Kamens (1996), An approach to studying the effects of organic composition on atmospheric aerosol photochemistry, *J. Geophys. Res.*, *101*(D14), 19,593–19,600.

Middlebrook, A. M., D. M. Murphy, and D. S. Thomson (1998), Observations of organic material in individual marine particles at Cape Grim during the First Aerosol Characterization Experiment (ACE 1), *J. Geophys. Res.*, *103*(D13), 16,475–16,484.

Monahan, E. C., D. E. Spiel, and K. L. Davidson (1986), A model of marine aerosol generation and wave disruption, in *Oceanic Whitecaps and Their Role in Air-Sea Exchange Processes*, edited by E. C. Monahan and G. MacNoicaill, pp. 167–174, Springer, New York.

Nagao, I., K. Matsumoto, and H. Tanaka (1999), Sunrise ozone destruction found in the sub-tropical marine boundary layer, *Geophys. Res. Lett.*, *26*, 3377–3380.

O'Dowd, C. D., and M. H. Smith (1993), Physico-chemical properties of aerosol over the North East Atlantic: Evidence for wind speed related sub-micron sea-salt aerosol production, *J. Geophys. Res.*, *98*, 1137–1149.

O'Dowd, C. D., M. H. Smith, I. E. Consterdine, and J. A. Lowe (1997), Marine aerosol, sea-salt, and the marine sulphur cycle: A short review, *Atmos. Environ.*, *31*, 73–80.

O'Dowd, C. D., M. C. Facchini, F. Cavalli, D. Cebrunis, M. Mircea, S. Decesari, S. Fuzzi, Y. J. Yoon, and J.-P. Putard (2004), Biogenically driven organic contribution to marine aerosol, *Nature*, *431*, 676–680.

Pierce, J. R., and P. J. Adams (2006), Global evaluation of CCN formation by direct emission of sea salt and growth of ultrafine sea salt, *J. Geophys. Res.*, *111*, D06203, doi:10.1029/2005JD006186.

Pszenny, A. A. P., J. Moldanová, W. C. Keene, R. Sander, J. R. Maben, M. Martinez, P. J. Crutzen, D. Perner, and R. G. Prinn (2004), Halogen cycling and aerosol pH in the Hawaiian marine boundary layer, *Atmos. Chem. Phys.*, *4*, 147–168.

Resch, F., and G. Afeti (1991), Film drop distribution from bubbles bursting in seawater, *J. Geophys. Res.*, *96*, 10,681–10,688.

Resch, F., and G. Afeti (1992), Submicron film drop production as a function of bubble size, *J. Geophys. Res.*, *97*, 3679–3683.

Rosen, M. J. (1978), *Surfactants and Interfacial Phenomena*, John Wiley, Hoboken, N. J.

Russell, L. M., and E. G. Singh (2006), Submicron sea salt production in bubble bursting, *Aerosol Sci. Technol.*, *40*, 664–671.

Saiz-Lopez, A., J. M. C. Plane, and J. A. Shillito (2004), Bromine oxide in the mid-latitude marine boundary layer, *Geophys. Res. Lett.*, *31*, L03111, doi:10.1029/2003GL018956.

Sander, R., Y. Rudich, R. von Glasow, and P. J. Crutzen (1999), The role of $BrNO_3$ in marine tropospheric chemistry: A model study, *Geophys. Res. Lett.*, *26*, 2858–2860.

Sander, R., et al. (2003), Inorganic bromine in the marine boundary layer: A critical review, *Atmos. Chem. Phys*, *3*, 1301–1336.

Schkolnik, G., D. Chand, A. Hoffer, M. Andreae, C. Erlick, E. Swietlicki, and Y. Rudich (2006), Constraining the density and complex refractive index of elemental and organic carbon in biomass burning aerosol using optical and chemical measurements, *EOS Trans. AGU*, *87*(52), Fall Meeting Suppl., Abstract A43A-0107.

Scott, J. C. (1986), The effect of organic films on the water surface motions, in *Oceanic Whitecaps*, edited by E. C. Monahan and G. M. Niocaill, pp. 159–166, Springer, New York.

Sievering, H., J. Cainey, M. Harvey, J. McGregor, S. Nichol, and P. Quinn (2004), Aerosol non-sea-salt sulfate in the remote marine boundary layer under clear-sky and normal cloudiness conditions: Ocean-derived biogenic alkalinity enhances sea-salt sulfate production by ozone oxidation, *J. Geophys. Res.*, *109*, D19317, doi:10.1029/2003JD004315.

Skop, R. A., W. G. Lindsley, and J. W. Brown (1991), Radiotracer studies of surfactant transport to the sea-air interface by submillimeter-size bubbles, *Exp. Fluids*, *10*, 251–256.

Smith, M. H., P. M. Park, and I. E. Consterdine (1993), Marine aerosol concentrations and estimated fluxes over the sea, *Q. J. R. Meteor. Soc., Part A*, *119*(512), 809–824.

Tanaka, P. L., et al. (2003), Direct evidence for chlorine-enhanced urban ozone formation in Houston, Texas, *Atmos. Environ.*, *37*, 1393–1400.

Tang, I. N. (1997), Thermodynamic and optical properties of mixed-salt aerosols of atmospheric importance, *J. Geophys. Res.*, *102*, 1883–1893.

Thorpe, S. A. (1982), On the cloud of bubbles formed by a breaking wind-wave in deep water, and their role in air-sea gas transfer, *Philos. Trans. R. Soc. Ser. A.*, *304*, 155–210.

Thorpe, S. A., and A. J. Hall (1983), The characteristics of breaking waves, bubble clouds, and near-surface currents observed using side-scan sonar, *Cont. Shelf Res.*, *1*, 353–384.

Thorpe, S. A., A. R. Stubbs, A. J. Hall, and R. J. Turner (1982), Wave-produced bubbles observed by side-scan sonar, *Nature*, *296*, 636–638.

Toumi, R. (1994), BrO as a sink for dimethylsulfide in the marine atmosphere, *Geophys. Res. Lett.*, *21*, 117–120.

Tseng, R.-S., J. T. Viechnicki, R. A. Skop, and J. W. Brown (1992), Sea-to-air transfer of surface-active organic compounds by bursting bubbles, *J. Geophys. Res.*, *97*, 5201–5206.

Turekian, V., S. A. Macko, and W. C. Keene (2003), Concentrations, isotopic compositions, and sources of size-resolved, particulate organic carbon and oxalate in near-surface marine air at Bermuda during spring, *J. Geophys. Res.*, *108*(D5), 4157, doi:10.1029/2002JD002053.

Turpin, B. J., and H. Lim (2001), Species contributions to $PM_{2.5}$ mass concentrations: Revisiting common assumptions for estimating organic mass, *Aerosol Sci. Technol.*, *35*, 602–610.

Vignati, E., G. de Leeuw, and R. Berkowicz (2001), Modeling coastal aerosol transport and effects of surf-produced aerosols on processes in the marine atmospheric boundary layer, *J. Geophys. Res.*, *106*, 20,225–20,238.

Vogt, R., P. J. Crutzen, and R. Sander (1996), A mechanism for halogen release from sea-salt aerosol in the remote marine boundary layer, *Nature*, *383*, 327–330.

von Glasow, R., and P. J. Crutzen (2004), Model study of multiphase DMS oxidation with a focus on halogens, *Atmos. Chem. Phys.*, *4*, 589–608.

von Glasow, R., R. Sander, A. Bott, and P. J. Crutzen (2002), Modeling halogen chemistry in the marine boundary layer: 2. Interactions with sulfur and cloud-covered MBL, *J. Geophys. Res.*, *107*(D17), 4323, doi:10.1029/2001JD000943.

Wallace, G. T., and R. A. Duce (1978), Transport of particulate organic matter by bubbles in marine waters, *Limnol. Oceanogr.*, *23*, 1155–1167.

Wilson, T. R. S. (1975), Salinity and the major elements of sea water, in *Chemical Oceanography*, vol. 1, 2nd edition, edited by J. P. Riley and G. Skirrow, pp. 365–413, Elsevier, New York.

Zhou, J., K. Mopper, and U. Passow (1998), The role of surface-active carbohydrates in the formation of transparent exopolymer particles by bubble adsorption of seawater, *Limnol. Oceanogr.*, *43*, 1860–1871.

E. E. Dahl, Chemistry Department, Loyola College in Maryland, Baltimore, MD 21210, USA.

A. J. Davis and D. J. Kieber, Chemistry Department, College of Environmental Science and Forestry, State University of New York, Syracuse, NY 13210, USA.

M. A. Izaguirre, Rosenstiel School of Marine and Atmospheric Science, University of Miami, Miami, FL 33149, USA.

W. C. Keene, M. S. Long, and J. R. Maben, Department of Environmental Sciences, University of Virginia, Charlottesville, VA 22904, USA. (wck@virginia.edu)

H. Maring, Radiation Sciences Program, NASA, Washington, DC 20546, USA.

A. A. P. Pszenny, Institute for the Study of Earth, Oceans, and Space, University of New Hampshire, Durham, NH 03824, USA.

R. Sander, Air Chemistry Department, Max Planck Institute for Chemistry, D-55020 Mainz, Germany.

L. Smoydzin, School of Environmental Sciences, University of East Anglia, Norwich NR4 7TJ, UK.

X. Zhou, Wadsworth Center, New York State Department of Health, and School of Public Health, State University of New York, Albany, NY 12201, USA.